Infrared Measurements of Pristine and Disturbed Soils 2. Environmental Effects and Field Data Reduction

Keith A. Horton,[*][†] *Jeffrey R. Johnson,*[*][‡] *and Paul G. Lucey*[*]

We have expanded on previous methods for correcting thermal infrared field measurements for atmospheric downwelling radiance (Salisbury and D'Aria, 1992; Korb et al., 1996; Hook and Kahle, 1996) by comparing the sensitivity of various input parameters (sample temperature, diffuse gold plate emissivity, and temperature) on this correction. We find that the sample temperature has the greatest influence on the applied atmospheric correction (cf. Nerry et al., 1990a,b; Labed and Stoll, 1991), and we present a method in which the sample temperature is varied to minimize the residual atmospheric emission lines in the measured field emissivity spectra. Direct comparison of laboratory hemispherical reflectance measurements of wet-sieved and dry-sieved samples with these appropriately corrected field observations of undisturbed and disturbed soils, respectively, provides a means to predict the expected infrared spectral contrast differences between such soils (see preceding article). ©Elsevier Science Inc., 1998

INTRODUCTION

An essential step in compositional remote sensing in the region of thermal emission is comparison of field and laboratory spectra. Laboratory spectra are often obtained using an integrating sphere to provide directional hemispherical reflectance, which Salisbury et al. (1994) showed could be used to derive emissivity via Kirchhoff's law within about 1%, despite the fact that, in the strictest

sense, the requirement of thermodynamic equilibrium in Kirchhoff's law is violated (Badenas, 1997).

Nerry et al. (1990a,b) and Labed and Stoll (1991) used the "emissivity box" approach (in which a large box surrounds a sample to allow control of the environmental radiation) to determine broad-band (8–14 μm) emissivities in the field and laboratory. Salisbury and D'Aria (1992), Korb et al. (1996), and Hook and Kahle (1996) presented field and computational methods for deriving spectral emissivity from field radiance spectra with supporting downwelling radiance measurements and radiometrically measured temperatures. These emissivity measurements, once corrected for environmental effects, can be directly compared to laboratory hemispherical reflectance measurements.

We have found that these methods are effective in reducing field measurements, but that the results are highly sensitive to the values of some of the input parameters, values which may not be well known, but also for many purposes not crucial in themselves. In this article, we summarize the general data reduction methodology used with the Designs & Prototypes FTIR field spectrometer (cf. Korb et al., 1996; Hook and Kahle, 1996) and evaluate how the individual input parameters (sample temperature, diffuse gold plate emissivity, and temperature) affect the correction of field data of soils to absolute emissivity. We find that the sample (target) temperature has the greatest influence on these corrections, consistent with the results of Nerry et al. (1990a,b) and Labed and Stoll (1991), who used different field measurement techniques and broad-band radiometers, and Rivard et al. (1995), who restricted their analyses to rocks.

Two soil examples, one from Ft. A.P. Hill, Virginia, and the other from Ft. Devens, Massachusetts, are presented to illustrate the results obtained. These particular sites were chosen from among those data sets in which

[*] Hawaii Institute of Geophysics and Planetology, University of Hawaii at Manoa, Honolulu
[†] Pacific Island Technology, Inc., Honolulu
[‡] Current address: U.S. Geological Survey, Flagstaff, AZ 86004

Address correspondence to K. A. Horton, Hawaii Inst. of Geophysics and Planetology, 2525 Correa Rd., Honolulu, HI 96822.
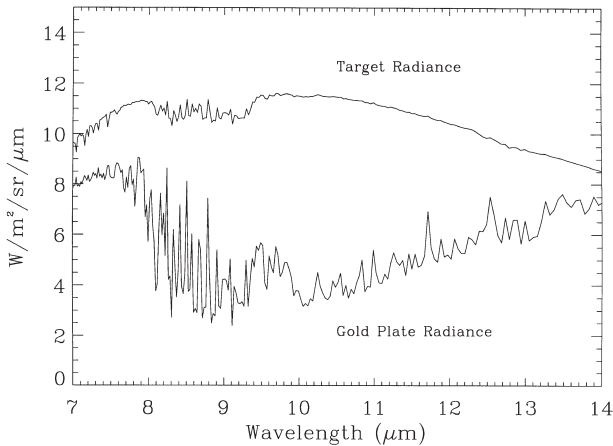
Figure 1. Calibrated radiance of undisturbed soil (target) and sky reflectance from a diffuse gold plate. Field data were acquired at Ft. Devens, Massachusetts.

both field and laboratory measurements have been completed. The geologic implications of these results and comparison of field measurements and laboratory spectra of samples returned from the field are explored in our companion paper (Johnson et al., 1998), also in this issue.

METHODOLOGY

All field experimental spectral data were collected with the Designs & Prototypes FTIR field spectrometer (Korb et al., 1996; Hook and Kahle, 1996; Ninomiya et al., 1997). Data were normally acquired with the instrument by co-adding 16 uncalibrated magnitude spectra for each measurement. Three to five spectra were taken per site. These measurements were taken usually at a distance of ~1.2 m from the target area. Additionally, data were acquired of a diffuse reflective gold plate in order to measure the downwelling radiance spectrum near the time of sample spectra acquisition (see Fig. 1). Temperatures of the target site and the gold plate were measured with a small, portable, broadband radiometer (Omegascope Model OS71), primarily because it allows a noncontacting first-order estimation of the target site temperature. The calibration blackbody temperatures were set to bracket the site temperature over a range of 35°C on average to minimize any system nonlinearities (cf. Korb et al., 1996). In the following sections, we describe the calibration of these data to total sensor-received spectral radiance (W/m²/sr/μm), apparent emissivity, and absolute emissivity corrected for downwelling radiance.

Radiometric Calibration

An instrumental count (DN) from the spectrometer is a function of at-sensor spectral radiance, $L(\lambda)$, and instrumental factors, such that

$$DN(\lambda)=R(\lambda)L(\lambda)+O(\lambda), \qquad (1)$$

where $O(\lambda)$ is a wavelength-dependent offset due to electronic factors and instrumental self-emission and $R(\lambda)$ is the spectral transmission efficiency or response. Mapping from DN to radiance can be performed by obtaining measurements of blackbodies at two different temperatures. Assuming detector linearity, the spectral response for a measurement can be calculated from two blackbodies, $DN_x(\lambda)$, as

$$R(\lambda)=\frac{DN_1(\lambda)-DN_2(\lambda)}{B(T_1,\lambda)-B(T_2,\lambda)}, \qquad (2)$$

where $B(T_x,\lambda)$ is the Planck blackbody spectral radiance of each calibration blackbody. Offset is calculated from either blackbody by

$$O(\lambda)=DN(\lambda)-R(\lambda)*B(T,\lambda). \qquad (3)$$

At-sensor measured target spectral radiance [$L_{meas}(\lambda)$] is then calculated by

$$L_{meas}(\lambda)=\frac{DN_{meas}(\lambda)-O(\lambda)}{R(\lambda)}. \qquad (4)$$

The measured scene radiance is, in reality, composed of the sum of radiances entering the instrument at the input optic, and includes the desired target radiance, reflected atmospheric downwelling radiance, and the direct path radiance of the atmosphere between the target and the sensor. The equation describing this relationship is given by

$$\begin{aligned} L_{meas}(\lambda)=&B(T_T,\lambda)\varepsilon_T(\lambda)\tau_P(\lambda)\\ &+ (1-\varepsilon_T(\lambda))\,L_{DW}(\lambda)\tau_P(\lambda)+L_P(\lambda), \qquad (5)\end{aligned}$$

where

$B(T_T,\lambda)=$Planck blackbody spectral radiance of the target at temperature T_T,
$\varepsilon_T(\lambda)=$spectral emissivity of the target,
$\tau_P(\lambda)=$path atmospheric spectral transmissivity between the target and instrument,
$L_{DW}(\lambda)=$downwelling hemispherical spectral radiance onto the target,
$L_P(\lambda)=$spectral radiance of the atmosphere path between the target and instrument.

The three terms on the right of Eq. (5) then represent: the spectral radiance received from the target, the downwelling spectral radiance reflected from the target to the sensor, and the direct spectral radiance of the intervening atmosphere between the target and sensor.

Considering that the instrument-to-target distance is on the order of 1 m, a MODTRAN 3 radiative transfer model approximating conditions during one of the field examples given here (Ft. Devens, Massachusetts) shows that within the wavelength range, 8–14 μm, the effects of atmospheric transmissivity [$\tau_P(\lambda)>0.99$] and path radiance [$L_P(\lambda)<0.5\%$ of total radiance] may be considered negligible, and Eq. (5) may then be simplified to
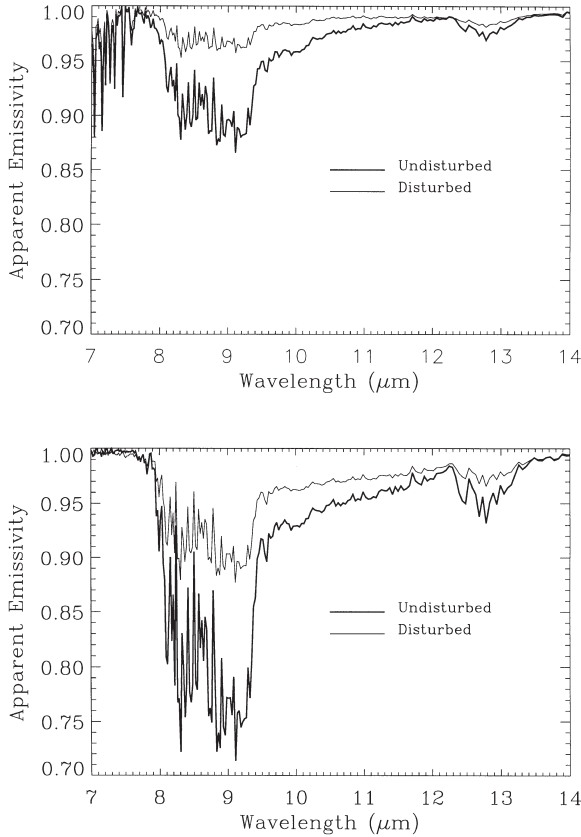
Figure 2. Apparent emissivities of disturbed and undisturbed soils at Ft. Devens, Massachusetts (top) and Ft. A.P. Hill (bottom). Note sharp atmospheric emission lines due to the downwelling radiance component, particularly in the reststrahlen bands near 9 μm.

$$L_{meas}(\lambda) = B(T_T, \lambda)\varepsilon_T(\lambda) + (1 - \varepsilon_T(\lambda))L_{DW}(\lambda). \qquad (6)$$

Figure 1 shows examples of spectral radiance data of undisturbed ground at Ft. Devens, Massachusetts and radiance from a diffuse gold reflector. Two examples of typical apparent emissivity spectra of disturbed and undisturbed soils are shown in Figure 2 (Ft. Devens, top; Ft. A.P. Hill, bottom). These spectra include reflected downwelling radiance, which must be removed to derive absolute emissivity, as described in the next section.

Downwelling Radiance Correction

We follow the example of Salisbury and D'Aria (1992), Rivard et al. (1995), Korb et al. (1996), and Hook and Kahle (1996) and use a diffuse reflecting gold plate to measure downwelling spectral radiance. Korb et al. (1996) and Hook and Kahle (1996) showed that the downwelling spectral radiance correction to the diffuse gold plate spectral measurement introduces a small error because the emissivity of the diffuse gold plate is not exactly 1.0. The downwelling spectral radiance measurement includes a term which incorporates thermal emission from the plate such that

$$L_G(\lambda) = \varepsilon_G(\lambda)B(T_G, \lambda) + (1 - \varepsilon_G(\lambda))L_{DW}(\lambda), \qquad (7)$$

where:

$L_G(\lambda)$ = measured spectral radiance from the diffuse gold plate,
$\varepsilon_G(\lambda)$ = spectral emissivity of the gold plate,
$B(T_G, \lambda)$ = Planck blackbody spectral radiance of the gold plate at temperature, T_G.

Rearranging Eq. (7), the downwelling spectral radiance, which is required in Eq. (6), is calculated from

$$L_{DW}(\lambda) = \frac{L_G(\lambda) - \varepsilon_G(\lambda)B(T_G, \lambda)}{1 - \varepsilon_G(\lambda)}. \qquad (8)$$

We measure the approximate temperature of the gold plate, T_G with a broadband radiometer observing the black back of the gold plate. The spectral reflectivity of the diffuse gold surface, $\rho_G(\lambda)$, is fairly flat, has been measured between 0.94 and 0.97 (Salisbury and D'Aria, 1992; Salisbury et al., 1994), and, according to Kirchhoff's law, results in a spectral emissivity of between 0.03 and 0.06. In the MODTRAN-3 1-m path example for Ft. Devens, emission from the plate results in an average 7% of the total radiance received at the sensor integrated over the 8–14 μm region.

Variations in measurements of downwelling radiance may occur due to any change within the reflective field of view of the sensor. Significant variations in downwelling radiance have been noted primarily only when clouds or man-made objects obscure the scene directly overhead. Although data presented here were acquired under relatively constant atmospheric conditions, we recognize that the effects of time variations between target and downwelling radiance measurements can significantly affect the ability of our technique to correct for the contribution of downwelling radiance to the calculation of absolute emissivity (Korb et al., 1996).

Absolute Emissivity Calculation

In order to calculate the absolute spectral emissivity corrected for reflected downwelling radiance, Eq. (6) may be rewritten as

$$\varepsilon_T(\lambda) = \frac{L_{meas}(\lambda) - L_{DW}(\lambda)}{B(T_T, \lambda) - L_{DW}(\lambda)}. \qquad (9)$$

Therefore, only the following three parameters must be either measured or estimated: the temperature of the target, the temperature of the gold plate, and the emissivity of the diffuse gold surface. The emissivity of the gold, as noted previously, has been measured in the laboratory, is spectrally flat, and can be incorporated as a scalar. In the field, both the temperatures of the gold plate and the ground surface are estimated from radiometer measurements.
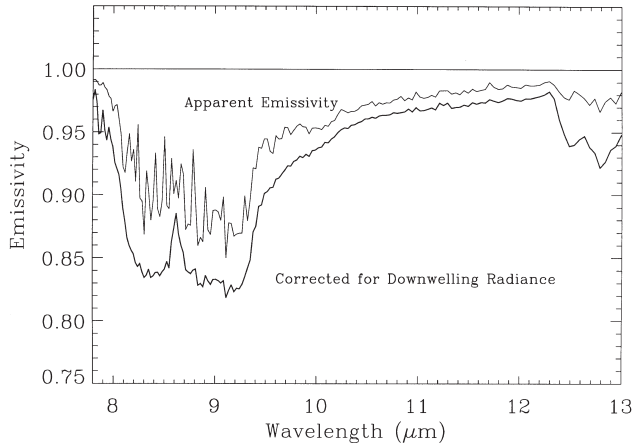
Figure 3. Plots of apparent emissivity and emissivity corrected for reflected downwelling radiance from an undisturbed soil surface at Ft. Devens, Massachusetts.

Figure 5. Plot showing the effects on derived absolute emissivity of a field spectrum by varying the temperature of the gold plate. The gold plate emissivity was held constant at 0.04, and the ground temperature held constant at 22.6°C.

Figure 3 is a plot of the uncorrected, or apparent emissivity of undisturbed soil from Ft. Devens shown in Figure 2 (top). In addition, shown in this plot is the emissivity corrected for reflected downwelling radiance calculated following the procedures outlined above and described below. The technique removes the sharp atmospheric emission lines contributed to the field measurement by downwelling radiance from the atmosphere reflected from the target surface and "fills in" the silicate reststrahlen doublet near 9 μm.

EFFECTS OF INPUT PARAMETERS

As pointed out, measurements or estimates of the temperature of the target, the temperature of the gold plate, and the emissivity of the diffuse gold surface are required for these corrections. By keeping the two required tem-

peratures constant and varying the gold emissivity, the effects of errors in the gold surface emissivity measurement can be shown. Figure 4 gives three plots of corrected target spectral emissivity for three different emissivity values for the gold surface. For this particular sample (Ft. A.P. Hill), the effect of varying the gold emissivity is only significant within the reststrahlen bands. By either halving (0.02) or doubling (0.08) the gold emissivity from our original estimate of 0.04, results in a band depth contrast of only ~1% or ~2%, respectively.

Due to the low emissivity of the diffuse gold plate, the effect of errors in the measurement of the gold plate temperature is minimal. Shown in Figure 5 are the results on target emissivity obtained by varying the gold plate temperature while holding the gold emissivity and

Figure 4. Plot showing the effects on derived absolute emissivity of a field spectrum by varying the diffuse gold reflector emissivity. The gold plate temperature was held constant at 28°C, and the ground temperature held constant at 22.6°C.
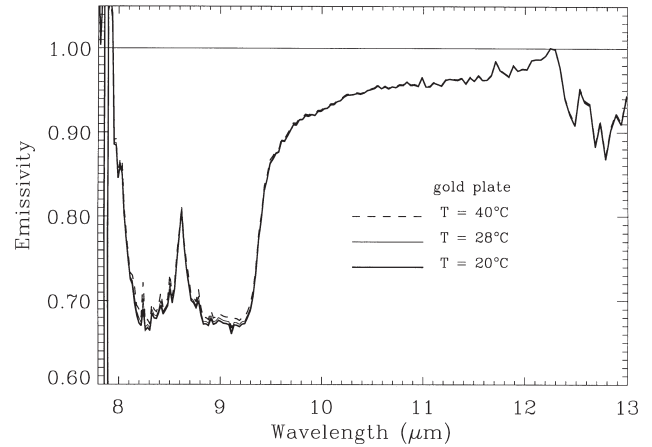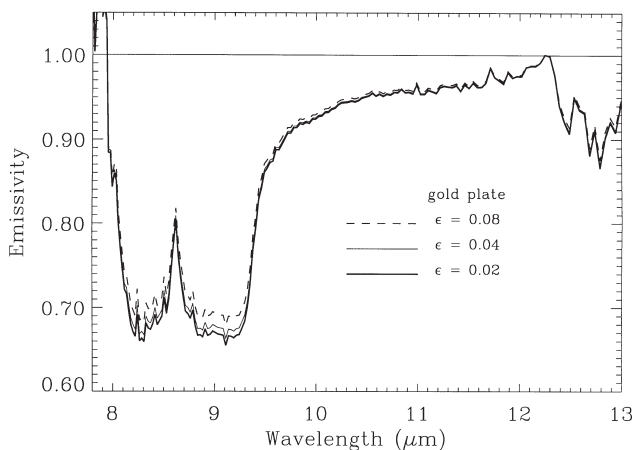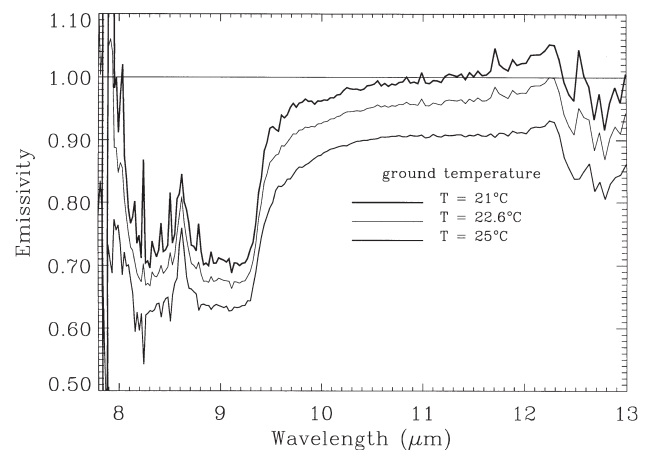

Figure 6. Plot showing the effects on derived absolute emissivity of a field spectrum by varying the target or ground temperature. The gold plate temperature was held constant at 28°C, and its diffuse surface emissivity held constant at 0.04. Each curve represents the best fit at each specific estimated ground temperature.
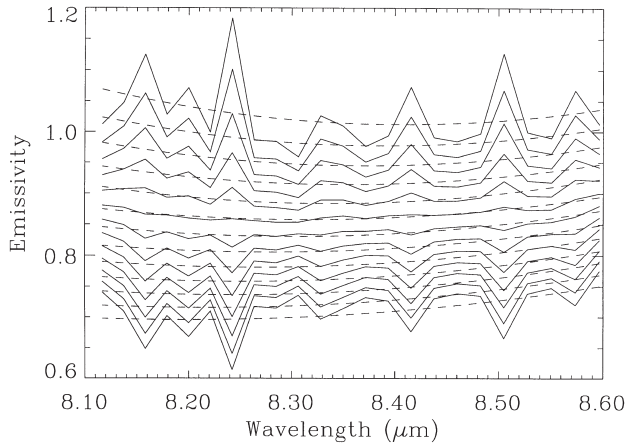
Figure 7. Derived absolute emissivity spectra (solid) for a range of target temperatures from 25°C (top curve) to 31°C (bottom curve) in 0.5°C increments. Superimposed on the emissivity spectra are the second-order best-fit curves (dashed) for these temperatures.

Figure 8. Emissivity residuals between derived absolute emissivity and best-fit curves as a function of temperature. Reflected atmospheric emission lines are minimized at a target temperature of 27.5°C.

ground temperature constant in Eq. (8) and (9). This plot demonstrates that a wide range of temperature estimates produce little variance in the final emissivity.

Errors in measurement of the ground surface temperature, however, can have a significant effect on the target emissivity calculation. Figure 6 plots the corrected emissivity results from varying the ground temperature estimation by approximately ±2°C while keeping the gold plate temperature and gold surface emissivity constant. Two important effects are noted when the ground or target temperature is incorrectly estimated: 1) The entire calculated spectrum is affected, not only the reststrahlen bands; and 2) the atmospheric emission lines are accentuated, either in the plus or minus direction. Our method uses as the objective function, the minimization of the reflected atmospheric emission lines within a portion of the measured spectrum (the short wavelength lobe of the silicate reststrahlen doublet between 8.12 mm and 8.60 μm). By fixing the diffuse gold plate temperature and emissivity, and varying only the target temperature, the spectrum is fit with a second-order polynomial as best representing the general shape of the reststrahlen lobe, and the residuals between the resulting emissivity spectrum and the second-order polynomial curve are calculated.

Figure 7 shows the calculated emissivity spectrum (solid) within this wavelength region for a range of target temperatures from 25°C to 31°C in 0.5°C increments. Superimposed on the emissivity spectra are the second-order best-fit curves (dashed). A plot of the emissivity residuals as a function of temperature is given in Figure 8 and shows that the atmospheric emission lines are minimized at a target temperature of 27.5°C for this example. From Figure 7 it can be seen that underestimating the ground temperature retains the atmospheric emis-
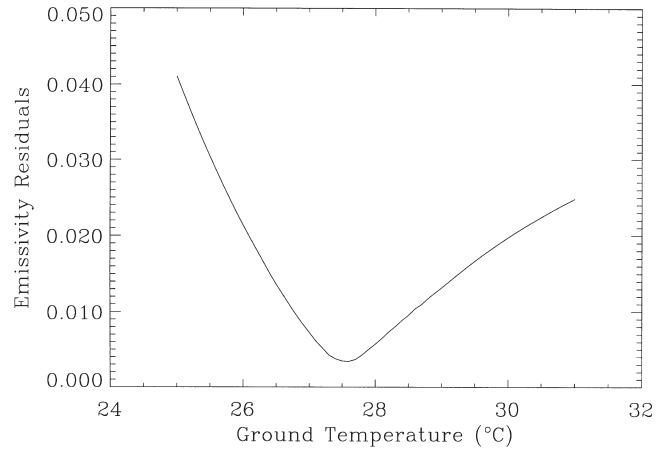
sion lines in the measured spectrum and, secondarily, results in too high an estimate of the overall spectral emissivity (>1.0). Overestimating the ground temperature produces low values of emissivity and reinserts, in an opposite sense, the atmospheric lines.

The ability of this method to recover accurate emissivities from field data is illustrated by Figure 9, which shows spectra of the same soils obtained in the field and in the laboratory. The top portion of Figure 9 shows spectra of disturbed (field emissivity—atmospheric emission lines minimized) and dry-sieved (laboratory hemispherical reflectance) soils overlain. The field spectrum shows slightly higher emissivity due to minor residual soil moisture in the overturned soil during data collection. The lower plot of Figure 9 shows that the spectra of undisturbed soil (field) matches that of the wet-sieved soil (lab).

CONCLUSIONS

The methods presented here offer significant promise of additional versatility in spectral measurements of soils in the thermal infrared. Field measurements required to obtain the data necessary to implement these techniques are straightforward and relatively easy to implement.

The effects of the various input parameters suggest that, particularly those due to uncertainties in the measurement of the target or ground temperature, the primary figure of merit in determining the quality and accuracy of the applied atmospheric correction is the minimization of the residual atmospheric emission lines in the measured emissivity spectra.

Direct comparison of hemispherical reflectance measurements of wet-sieved and dry-sieved samples versus undisturbed and disturbed soils, respectively, may provide a means to predict the expected discrimination perfor-
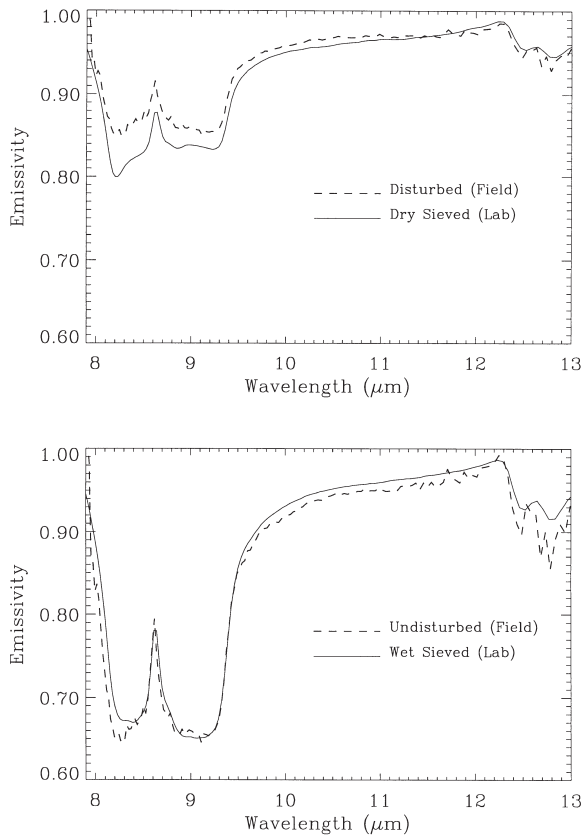
Figure 9. Upper: Spectra of disturbed (field emissivity—atmospheric emission lines minimized) and dry-sieved (laboratory hemispherical reflectance) soils overlain. The field spectrum of the disturbed soil shows higher emissivity due to moisture in the recently overturned soil. Lower: Spectra of undisturbed soil (field) with wet-sieved soil (lab).

mance of infrared spectral contrast measurements for soils (cf. Johnson et al., 1998).

In conclusion, we have shown that the previously published methods work well, but care must be taken to choose the critical ground temperature when reducing field radiance measurements to emissivity (cf. Salisbury et al., 1994; Nerry et al., 1990a,b; Labed and Stoll, 1991; Rivard et al., 1995). Precise gold plate temperature and emissivity are not critical because of the generally low value of emissivity. We have shown that a second-order polynomial fit of the 8.12–8.60 μm region can be used to construct an effective objective function to optimize the target temperature to remove atmospheric emission lines and recover spectral contrast.

REFERENCES

Badenas, C. (1997), Comments on Kirchhoff's law in thermal-infrared remote sensing. *Int. J. Remote Sens.* 18:229–234.

Hook, S. J., and Kahl, A. B. (1996), The micro Fourier transform interferometer (μFTIR)—a new field spectrometer for acquisition of infrared data of natural surfaces. *Remote Sens. Environ.* 56:172–181.

Johnson, J. R., Lucey, P. G., Horton, K. A., and Winter, E. M. (1998), Infrared measurements of pristine and disturbed soils. 1. Spectral contrast differences between field and laboratory data. *Remote Sens. Environ.*, this issue.

Korb, A. R., Dybwad, P., Wadsworth, W., and Salisbury, J. W. (1996), Portable Fourier transform infrared spectroradiometer for field measurements of radiance and emissivity. *Appl. Opt.* 35:1679–1692.

Labed, J., and Stoll, M. P. (1991), Spatial variability of land surface emissivity in the thermal infrared band: Spectral signature and effective surface temperature. *Remote Sens. Environ.* 38:1–17.

Nerry, F., Labed, J., and Stoll, M. (1990a), Spectral properties of land surfaces in the thermal infrared 1. Laboratory measurements of absolute spectral emissivity signatures. *J. Geophys. Res.* 95:7027–7044.

Nerry, F., Labed, J., and Stoll, M. (1990b), Spectral properties of land surfaces in the thermal infrared 2. Field method for spectrally averaged emissivity measurements. *J. Geophys. Res.* 95:7045–7054.

Ninomiya, Y., Matsunaga, T., Yamaguchi, Y., et al. (1997), A comparison of thermal infrared emissivity spectra measured *in situ*, in the laboratory, and derived from thermal infrared multispectral scanner (TIMS) data in Cuprite, Nevada, U.S.A. *Int. J. Remote Sens.* 18:1571–1581.

Rivard, B., Thomas, P. J., and Giroux, J. (1995), Precise emissivity of rock samples. *Remote. Sens. Environ.* 54:152–160.

Salisbury, J. W., and D'Aria, D. M. (1992), Infrared (8–14 μm) remote sensing of soil particle size. *Remote Sens. Environ.* 42:157–165.

Salisbury, J. W., Wald, A., and D'Aria, D. M. (1994), Thermal-infrared remote sensing and Kirchhoff's law 1. Laboratory measurements. *J. Geophys. Res.* 99:11,897–11,911.